Institut polytechnique de Grenoble - CERN

Master of Science in Nuclear Energy and Materials for Nuclear Engineering

MASTER THESIS

Studies on gas system upgrades for the CMS RPC detectors at CERN

Candidate:
Mattia **Busato**

Supervisor:
Prof. Emilie **Ferrié**
CERN Supervisor:
Beatrice **Mandelli**

Date: 13/09/2021
Academic Year: 2020/2021

Contents

List of Figures

[utf8]inputenc [main.tex]subfiles

Abstract

This master thesis work focused on the upgrade of the gas system of the RPC detector in the CMS experiment at CERN. Since these gaseous detectors are connected to the gas system with extremely fragile elements it is matter of fundamental importance maintaining a stable pressure in the detectors to avoid rupture of these components. To do so, an automatic regulation valve was added on each output line serving from 13 to 26 detector chambers. However, since these lines present pretty different pressure and flow-rate conditions the seat of each valve has been customized. To find the right geometry of the seat both simulation studies and experiments have been performed. The simulations were carried out using the commercial software ANSYS while experimental data were taken both using a laboratory set-up and modifying several lines on the actual experiment. Results from the simulations were compared with the hands-on test results and 4 different seat geometries were designed and studied assuring they could work with the required conditions. The seats have been 3D printed and the installation of these regulation valves on the system is foreseen for November 2021 in order to be ready for the next LHC run.

Chapter 1

High Energy Physics at the LHC

Particle Physics research aims to determine the fundamental matter components, their properties, and the way they interact with each other. The Standard Model (SM), that describes elementary particles and their interaction, has been successfully tested by the Physics program taking place at the Large Hadron Collider (LHC), especially with the discovery of the Higgs boson. Nevertheless, the SM shows some limitations that give rise to the need of exploring new physics beyond it. This chapter will illustrate the basics of elementary particles research and how it is approached at the LHC.

1.1 The Standard Model

The Standard Model contains the theoretical elements of modern Particle Physics described through the gauge invariance principle in the framework of quantum field theory. In the SM, the fundamental constituent of matter are 12 elementary particles called fermions, identified by their spin equal to 1/2. Fermions are divided into two types, leptons, and quarks, each type divided in turn into three generations. Charged leptons are electrons e^-, muons μ^- and taus τ^-, with their associated neutrinos (ν_e, ν_μ and ν_τ). Quarks are divided into first (u, d), second (c, s), and third (t, b) generations. The stable matter is made of fermions of the first generation. A table presenting the standard model of particle physics is shown in Fig. 1.1. Fermions interact through the exchange of spin-1 particles, the so-called gauge bosons, elementary particles

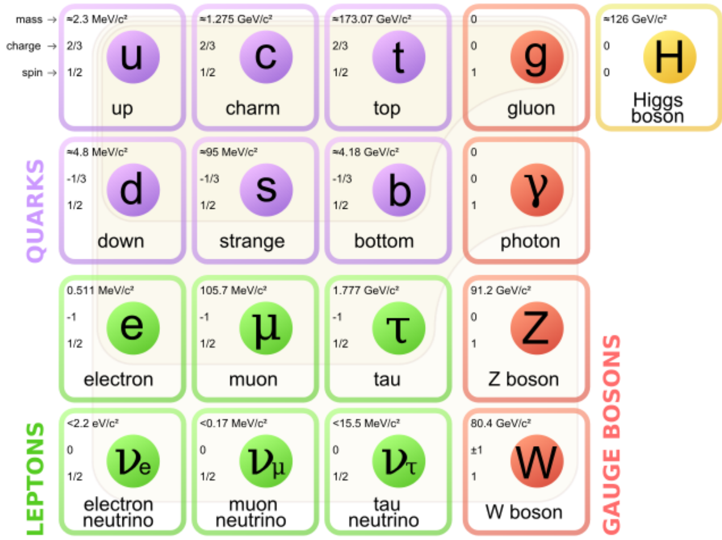

Figure 1.1: The Standard Model of Particle Physics [1].

themselves. These particles are associated with the fundamental interacting forces, and to the coupling constants that refer to their strength. The Electromagnetic interaction, described by Quantum Electro-Dynamics (QED), applies to all charged particles and it is mediated by the neutral boson g. The Weak interaction is mediated by the charged bosons W and Z, and it was unified with the Electromagnetic interaction by the ElectroWeak theory (EW). The strong interaction only applies to quarks, it is carried by eight gluons that can interact with each other and it is described by the Quantum Chromo-Dynamics theory (QCD). Nevertheless, the EW theory does not foresee a mechanism that gives mass to fundamental particles. The Brout-Englert-Higgs mechanism was therefore introduced to generate the mass of heavy bosons, and it can be applied to fermions too. Since the W and Z bosons are massive while the photon is not, the EW symmetry is broken, yielding to the existence of an additional scalar boson with spin 0, the Higgs boson. Its interaction with ordinary particles generates their masses, while its mass is an open parameter of the theory. Many SM parameters were successfully measured in the last decades, in a very large energy range and with high precision. However, the SM cannot be considered an ultimate theory, as many aspects still do not find an explanation in this model. It can somehow be seen as an approximation of a wider unified theory, which could include the description of aspects like the existence of the fourth elementary interaction (gravitation), the CP symmetry violation, the dark matter existence, and many others. One of the possible models could be the Super Symmetry (SUSY) theory, in which each particle of the SM has a super-symmetric partner with the same quantum numbers but the spin, which differs by 1/2. None of the proposed theories has so far found strong proofs in experimental observation, and the search for a unified theory remains therefore open.

1.2 Overview of the physics at LHC

The Large Hadron Collider (LHC) is a two-ring superconducting hadron accelerator and collider at the European Organization for Nuclear Research (CERN). Made of 27 km of superconducting magnets, laying 100 m underground, it allows the confinement and acceleration of two proton beams, running in opposite directions. It has been designed to provide enough statistics to fulfill the requirements of the CERN Physics program, oriented to precision measurements of the Standard Model as well as to the search for new physics. The LHC can nominally provide center-of-mass energy of 14 TeV for proton-proton collisions. Primary protons are obtained from Helium, and they are accelerated in a first linear accelerator (LINAC), to be then injected in the chain of circular accelerators that allows the achievement of their maximum energy (6.5 TeV). The LHC is also capable of providing heavy ions beams, supplying p-Pb and Pb-Pb collisions with a center-of-mass energy of 2.76 TeV and 5.02 TeV respectively. Fig. 1.2 reports a schematic drawing of the LHC complex with the different accelerators and experiments. The high center-of-mass energy allows the production of massive particles, and the high luminosity gives access to rare phenomena. Collisions happen in the four LHC Interaction Points, where the experiments are located. Two general-purpose Experiments, ATLAS (A Toroidal LHC ApparatuS) and CMS (Compact Muon Solenoid), were designed to explore all the possible aspects of the LHC physics, from heavy ions collisions and forward physics to Higgs boson physics and direct search of new particles. The ALICE experiment (A Large Ion Collider Experiment) is specifically dedicated to heavy ions physics, while the LHCb has the aim to maximize the LHC potential in beauty and charm physics. Though the final purpose is specific for each Experiment, the requirements on the detectors of which they are composed are quite the same. Their key aim is to identify charged particles and measure particles' momentum with high resolution. In addition, they all need

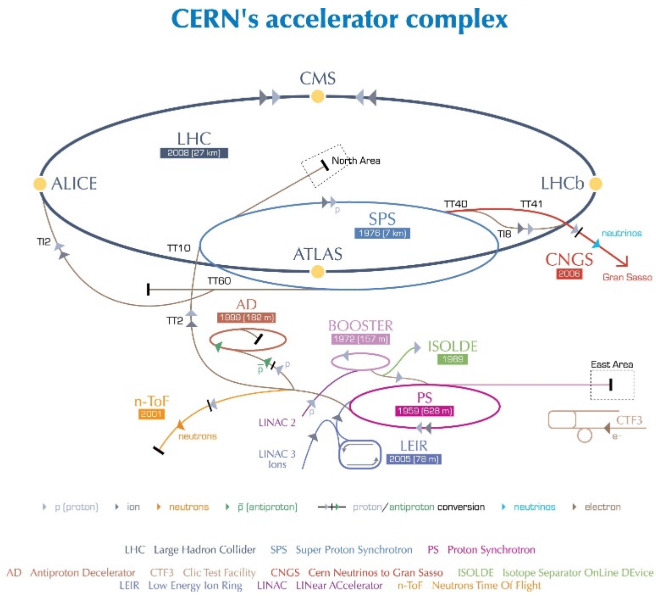

Figure 1.2: CERN's accelerators complex [2].

high granularity, to reduce the influence of overlapping events, and fast and radiation-tolerant electronics for proper data acquisition. LHC Experiments can be described dividing their structure into three different categories:

- **Inner detectors:** Located close to the collision points, they allow the tracking and momentum measurement of charged particles, as well as Interaction Point and vertices reconstruction.
- **Hadronic and Electromagnetic Calorimeters:** They measure the energy of hadrons, photons, and electrons crossing their volume, based on the energy loss of emerging particles.
- **Muon systems:** Since muons escape the electromagnetic calorimeter, a dedicated Muon system is used to detect them. Typically placed at the outermost layers of the experiments, it allows to unambiguously detect the signature of many relevant events [3].

Chapter 2

Gaseous detectors and gas systems at the LHC

In the framework of the LHC Physics program, muon detection is fundamental for the complete identification and characterization of collisions, since muons represent a very clean probe for many events of interest. Since muons have a mass of 105.6 GeV, they can easily penetrate matter and escape electromagnetic calorimeters. Every LHC experiment is equipped with a muon detector system, composed of dedicated detectors capable of identifying and tracking these particles. Gaseous detectors are the designed detector type for muon detection, therefore their working principle will be illustrated in this Chapter, with a focus on Resistive Plate Chambers (RPC). The LHC muon system infrastructure will also be described, giving an introductory overview of LHC gas systems design.

2.1 Working principles of gaseous detectors

When a fast-charged particle passes through a gas it can ionize molecules along its path, resulting in an ion pair, i.e. an ion and a free electron. Ion pairs are the basic constituent of the electrical signal developed in gaseous detectors. The ionization process occurs when a given amount of energy is transferred to the gas molecule by the incoming charged particle. However, energy-loss mechanisms may take place, such as excitation processes, in which an electron is not removed from the atom but just elevated to a higher bound state. For this reason, the W-value is defined as the average energy lost by the incident particle per ion pair formed, which is always greater than the simple ionization energy. The W-value strongly depends on the gas involved, the type of radiation, and its energy. Typical values are between 25 eV and 35 eV per ion pair.

Positive ions and free electrons created by the incoming particle would take part in the random thermal motion of the gas, with the tendency of moving away from regions of high density. Since electrons have a higher thermal velocity this process is much more pronounced for these particles. Of the many collision processes that can take place between free electrons, ions, and neutral gas molecules, the most significant ones for gaseous detector operation are charge transfer and recombination. However, the influence of both phenomena is decreased by applying an external electric field that enhances charges mobility and collection. The electric field will tend to move charged particles away from the point where they are generated, resulting in a motion that consists of the superposition of their random thermal velocity and their drift velocity in the field direction, with positive ions and free electrons moving in opposite directions. Their velocity is defined by $v = mE/p$ where E is the electrical field strength, p is the gas pressure and m is the mobility coefficient which remains basically constant over wide ranges of electric field and pressure. However, this coefficient is 1000 times greater for electrons than for ions.

If the electric field applied in the gas volume is low, electrons and ions created by incident radiation would simply drift while colliding with the gas molecules without producing any reaction until their collecting electrodes. However, when the applied field is increased to a certain value, the multiplication process starts to take place. Free electrons are accelerated by the electric field, rapidly gaining kinetic energy. When such energy is greater than the W-value of the gas molecules, secondary ionization can occur in the collision between free electrons and neutral gas molecules, generating new ion pairs. The average energy gained by free electrons increases with increasing electric field intensity, with a threshold value of the field above which secondary ionization can take place (around 106 V/m). The electrons produced from secondary ionization will in turn be accelerated by the field, undergoing collisions during the subsequent drift and thus creating additional ionization pairs. The gas multiplication process takes the form of a cascade, the so-called Townsend avalanche.

As reported in Fig. 2.1 it exists a region of the applied voltage for which the collected charge begins to multiply, and the avalanche amplitude increases (proportional region). Over this region, the gas multiplication factor is linear, and the amount of collected charged particles is proportional to the number of original ion pairs created by the incident radiation. Gas-filled proportional counters normally operate in this region of proportionality.

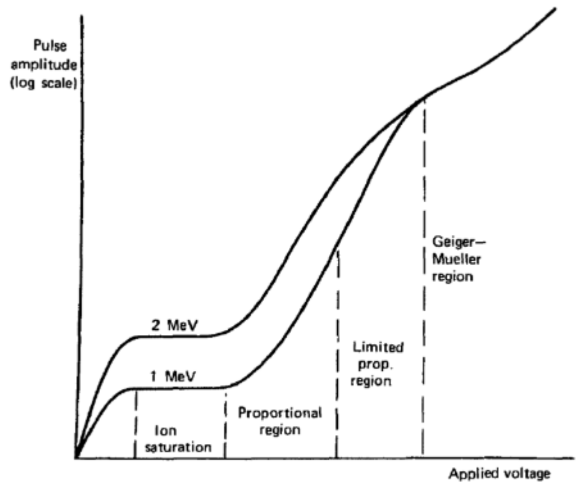

Figure 2.1: Regions of operation of gaseous detector, represented in terms of proportionality between the pulse amplitude and the applied voltage [4]

Gaseous detectors generally aim to work in the proportional region as the proportionality between the final number of electrons and the number of ion pairs created leads directly to proportionality with the energy lost by the incoming charged particle. Measuring the collected charges and counting the number of incoming particles allows therefore to have a measurement of such energy. The charge collection takes place by the formation of a signal on the electrodes which, in the most basic configurations, are the same that allow establishing the electric field in the gas volume through a given voltage difference. The signal generation rises from the induced charge on the electrodes by the movement of ions and electrons, where electrons are typically chosen as the main collected charges thanks to their higher drift velocity. The induced charge variation along the time of displacement of the electron towards the electrode is described by the expression of the voltage as a function of time, which therefore defines the time development of the signal depending on the specific electric field shape [3].

2.2 Resistive plate chambers

Resistive Plate Chambers (RPC) are gaseous parallel-plate detectors characterised by a fast time resolution (around 1 ns) and a good space resolution (around 1 cm). For this reason, they are well suited for space-time particle tracking as required for the muon trigger at the LHC.

RPCs are composed of two parallel plates made of bakelite with a bulk resistivity of $10^{10} - 10^{11} \Omega cm$, separated by a gas gap of few millimeters. The chamber is gas-tight and it is attached through input/output connectors to a gas system that constantly refreshes the gas mixture. The outer surfaces of the resistive material are coated with conductive graphite paint to form the HV and ground electrodes. The read-out is performed by means of aluminum strips separated from the graphite coating by an insulating PET film [x]. In Fig. 2.2, a schematic view of a RPC is reported.

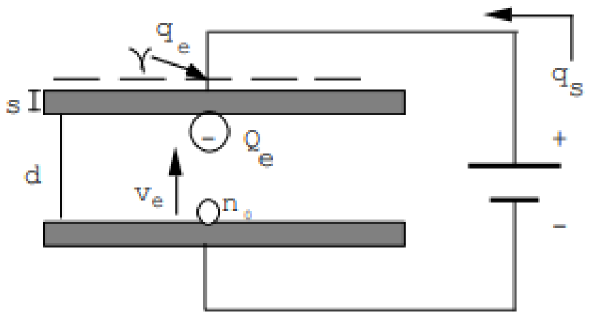

Figure 2.2: Schematic representation of an RPC detector working principle [5].

As reported in the schematic above, when a cluster of n_0 electrons produced by an ionizing particle ignites the avalanche multiplication, an electronic charge Q_e is developed inside the gas gap. The drift of such charge towards the anode induces in the strips the charge q_e which is then read-out resulting in the signal of the RPC.

Regarding the gas used for this type of detector, there are few parameters to be taken into consideration. In general, the gas mixture should have a good combination of the following characteristics:

- High density of primary ion-electron clusters so that a high detection efficiency is ensured;

- Being electronegative to reduce the spatial distribution of the discharge;
- Being not toxic or not dangerous for human health;
- The chemical process taking place inside the gas gap should not produce elements that can damage the electrode surface.

The most common gas used to meet the high density of ion-electron clusters requirement is $C_2H_2F_4$. In addition, a small percentage of SF_6 is employed due to its high electronegativity. Moreover, it should be taken into account that collisions between electrons and neutrals may give rise to excitation processes. The excited molecules would decay to their ground state, through the emission of a photon, which may create additional ionization elsewhere in the gas. These events are normally undesirable since they may cause a loss of proportionality. To suppress this process a small concentration of iC_4H_{10} is added to the mixture [6].

2.3 The LHC gas systems

As the gas mixture is the key element of gaseous detectors operation, a correct and stable mixture composition is a basic requirement for good and stable long-term performance. Therefore, the gas distribution system represents one of the most critical infrastructures to build and maintain. The basic function of the gas system is mixing the different gas components with precise proportions and delivering the mixture to the corresponding detectors at a stable pressure and flow rate. More than 30 dedicated gas systems are currently operational at CERN, over the four LHC Experiments as well as on other non-LHC experiments.

The LHC gas systems have been implemented following a modular design, in a way to be able to adapt to each detector type while maintaining a basic common structure. In this way, it was possible to optimize the building, commissioning, and maintenance operations of the system. Each of the modules complies with a specific function, and it is associated with a Programmable Logic Controller (PLC) unit, an industrial PC with basic functionalities for managing and monitoring the unit. The control software for the gas system runs in the PLC, which is connected to each gas system module to collect I/O information. The control software is based on the WinCC-OA SCADA tool and it keeps track of all the data from all the devices of the system.

Relevant parameters can be stored in a database and consulted through a custom graphical user interface. Such interface also allows to actively control the device, and more in general the gas system module with all its elements and in terms of interactions between two modules.

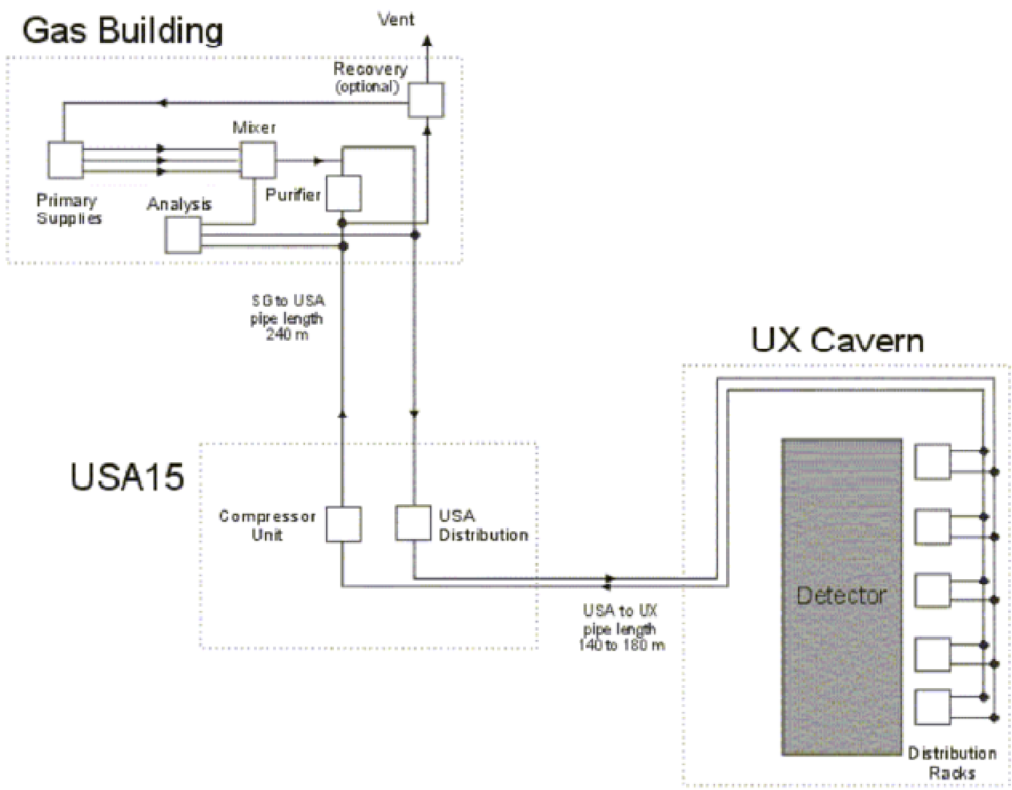

Figure 2.3: Schematic representation of the basic modules of an LHC gas system.

In the LHC Experiments, the gas system modules are located over three different levels: the surface room (SG), the underground service room (US), and the experimental cavern (UX). All the units that need immediate access are located in the SG, together with the primary gas supply. Following a route of a hundred meters, gas pipelines are brought underground to the US, which provides gas pre-distribution into several channels, as well as part of the gas system parameters regulation. The effective detailed distribution to each detector is instead done in the UX, from the service balcony gas racks.

Fig. 2.3 shows a schematic representation of the basic configuration of an LHC gas system, with the location of the single modules, briefly described in the list below.

Primary Gas Supply

Each gas is provided by two independent supply sources, one in use and one in stand-by, that can compensate when there is a failure in the other one or during replacement of the storage tanks.

Mixer Module

Primary gases are used to prepare the gas mixture for each detector. Mixer modules have up to four input lines, equipped with Mass Flow Controllers (MFCs), controlled via the software control system to set the correct proportion of each component of the gas mixture. For each gas line, two MFCs are installed with different volume flowrate ranges, in order to adapt to the needs of the gas systems in different operational conditions (run, fill, and purge). The uncertainty on the gas mixture concentrations is less than 1%. A mixing volume allows to properly mix the gas mixture components before it is sent to the following modules.

Gas Distribution

Several steps are needed to distribute the gas mixture to each detector, with specific and stable gas volume flow and pressure. Pre-distribution modules are located in the US, and they are related to different detector sectors of the experiment. They can be grouped with common regulation parameters, and then be split into smaller modules for specific sections of the detector sector. The gas is sent from the US to the UX, where the final distribution modules are located, and each pre-line is split into several smaller lines, to distribute the gas with the required granularity. The UX modules are designed with simplified electronic and manual systems which do not require access during LHC operation, while the others distribution levels can still be accessed and controlled during LHC runs if necessary. The gas mixture coming from the chambers is re-grouped into distribution and pre-distribution return modules.

Pump Module

Once the gas has flown from the UX into the return modules, the total gas flow rate is sent to the pump module that compresses the gas to higher pressure in order to send it back to the surface. In general, more pumps are present in a single module, to have a backup available or to increase the compressing rate.

Exhaust Module

The gas returning to the surface modules can either be fully exhausted to the atmosphere or sent back into the system, depending on the mode of operation. The return gas passes through the exhaust module, where pressure regulations control the gas emission in relation to the gas system parameters which are subject to specific requirements, as, for example, the chambers pressure stability.

Purifier Module

If the return gas is re-injected in the system, a purifier module allows acting on some of the impurities typically accumulated along the gas' path. Impurities can indeed accumulate due to leaks, gas supply quality, and detector permeability, or in some cases, they can directly be created inside the detector volume due to chemical reactions between the gas molecules and detectors material when subject to irradiation. The most common impurities are N_2, O_2 and H_2O, but only the last two can be easily removed through adsorption filters. The purifier module consists of two 24-liters volumes, filled with a specific material that reacts with the impurities. Molecular sieves are used for H_2O removals and metallic catalysts for O_2 absorption. As the active materials are subject to saturation, their usage is bound to regeneration cycles realized by heating up the volumes. The presence of two volumes allows one to have one in use while the other is regenerated, avoiding interrupting the purification process.

Gas Analysis Module

The gas analysis module allows continuous monitoring of the gas mixture quality in the critical gas system points (after mixer, exhaust, after purifier). Normally, O_2, H_2O, and InfraRed (iC_4H_{10}, CO_2) analysers are present, to measure the concentration of impurities and relevant mixture components. In some cases, the analysis module has an integrated system to perform gas chromatography analysis on selected sample lines obtaining a more complete measurement of all the gas mixture components.

In the simplest gas system operation mode, the gas mixture is sent underground to gas distribution and to the chambers, and once it is brought back on the surface, it is exhausted in the atmosphere. However, already in the first phases of LHC gas systems design, the possibility of re-using the gas mixture was taken into account in case of large detector volumes or usage of expensive gases to limit their consumption. When a gas system is operated in re-circulation mode, the gas mixture is collected after being used in the detector and undergoes purification processes to be then re-injected in the system. Operating the gas systems in a closed-loop allows to re-use a great fraction of the gas mixture. However, such operation mode implies a greater level of complexity of the gas system, as flow-rates and pressures need to be constantly regulated [3].

2.4 The RPC distribution module

Since the studies reported in this thesis are focused on the distribution module of the CMS RPC gas system, a more detailed overview on this module is given in the following. When the total volume flow coming from the mixer gets to the service gas room it is split by 3 distribution modules into 28 lines which bring the gas into the 6 main sectors of the detector complex: the barrel sector (upper and lower part) and the two endcap sectors (upper and lower parts). Therefore, each group of 4-5 lines reaches the 6 distribution modules in the experimental cavern where a second division of the flow lines takes place. Each line is split in several channels which finally deliver the gas mixture to each chamber. In Fig. 2.4 the Piping and Instrumentation Diagrams (P&IDs) of the distribution and pre-distribution modules of one group of lines are reported. At the input of each group there is a pressure regulator which make sure each line works at the required pressure. Once the flow is split it encounters a pneumatic valve, which is used in case there is the necessity of stopping the line for maintenance. A rotameter is used to manually regulate the flow-rate of the line, and finally a double bubbler is used as safety device in case the line's pressure decrease or increase over certain limits. The flow of each line is then split into channels going to the chambers. Before the chamber is placed a flow controller which regulate the flow. While after the chamber is placed a flow meter which measure the flow. These two devices are necessary to evaluate the leaks over the chamber. The channels are then collected by each line. The flow encounters again a double bubbler and a pneumatic valve for the same reasons as before. Moreover, a manual regulation valve is placed for a finer regulation of the chambers pressure. Each line converges into the group line proceeding towards the pump module. Each group line is regulated by an automatic regulation valve which decreases the effect of system perturbations on the chambers.

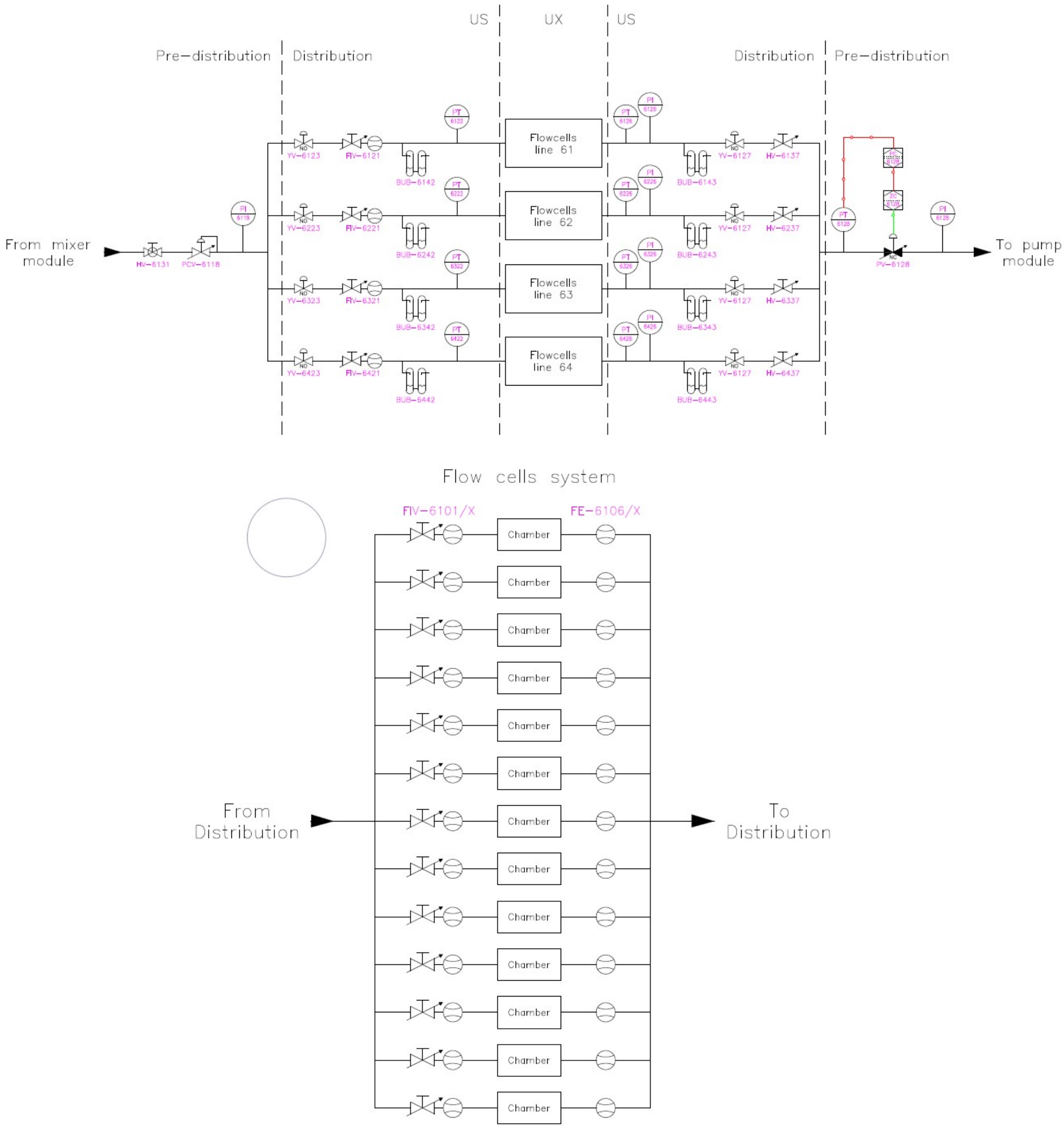

Figure 2.4: Pre-distribution and distribution modules P&ID (Group line 61).

Chapter 3

Studies on the regulation valves for the CMS RPC gas distribution system

In 2018 the second Run of the LHC has come to an end and the next run has been foreseen for 2021 (then postponed to 2022 due to the current Covid pandemic emergency). This long shut down has been dedicated, and it is currently dedicated, to the upgrade of the systems and the development of new devices for LHC. Regarding the LHC gas systems, some upgrades have been planned. Among the others, it was decided to add an automatic regulation valve at the output of each distribution line in the CMS RPC gas system in order to keep the chambers' pressure more stable (at the level of 0.1 mbar) and to simplify the operation of the system. In the following chapter, an introduction to the problem has been given as well as, an explanation on why such an upgrade is needed. The studies performed on the gas system are presented and the results are shown.

3.1 Introduction to the problem

CMS is made of different particle detectors including the RPCs. In Fig. 3.1 a 3D model of the experiment is shown. It can be noticed that the RPCs present in the experiment are spread at different heights in both barrel and endcap regions which are respectively the left and right caps and the central region around the collision point.

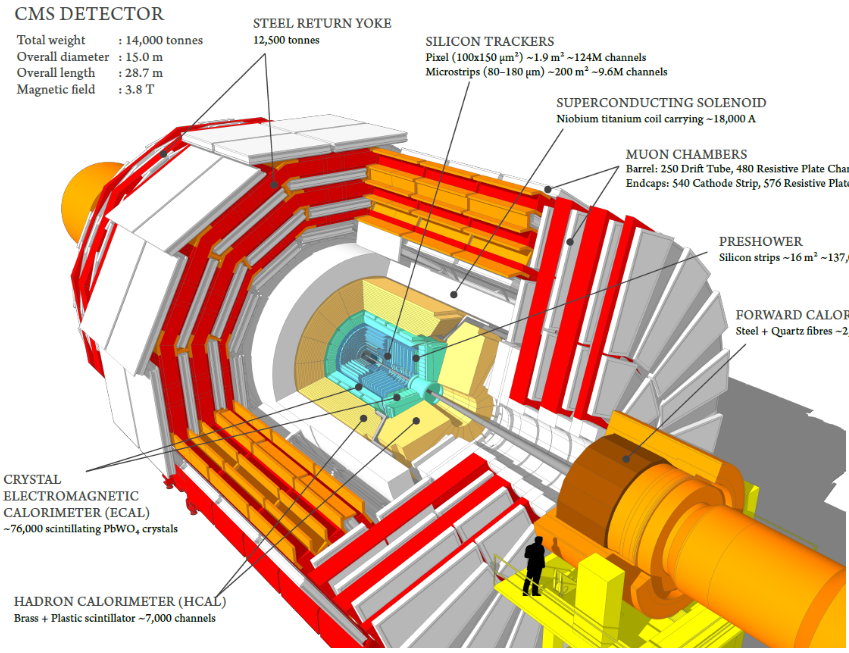

Figure 3.1: 3D model of the CMS experiment complex [7]

Since the RPCs gas connectors and connecting pipes are extremely fragile and difficult to repair or substitute due to limited access, it was decided to add an automated regulation valve on each return gas line, right before the pre-distribution modules. The regulation valve is programmed to keep the detector chamber's pressure as stable as possible. To do so, a pressure transmitter constantly measures the chamber's pressure, and through an electric motor, the valve adjusts its impedance accordingly. In order to produce the impedance needed for certain conditions, the seat of the valve can be customized. Among the different commercial options for this kind of valve, taking into consideration costs and space occupation, the ECONEX valve was chosen. In (Fig. 3.2) a photo of the valve is shown while in Fig. 3.3 the control software is showing an example of one CMS RPC distribution module. It is possible to see that the valve is set to keep the chamber's pressure at 0.1 mbar and that, at about 460 l/h, the valve's position is about 55%.

In the following studies, the process to design the seat is explained and different seat's geometries are compared.

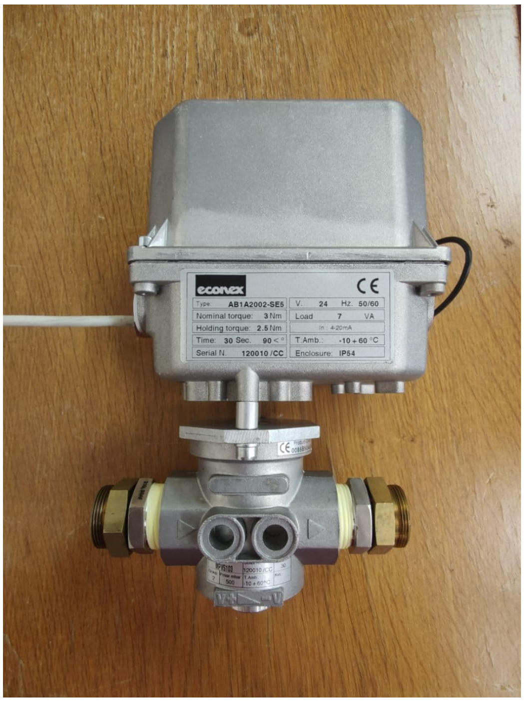

Figure 3.2: Automatic regulation valve from ECONEX.

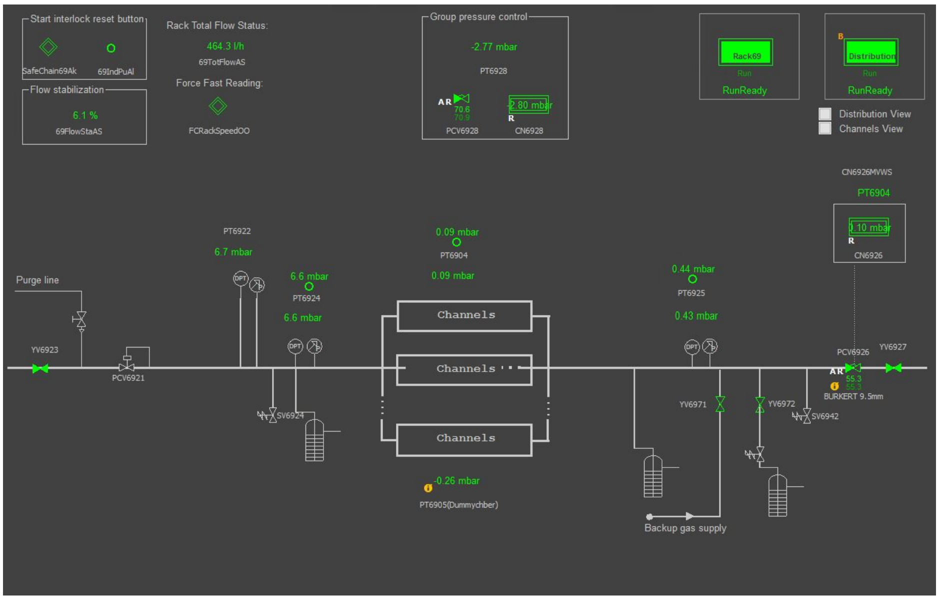

Figure 3.3: Control software showing an example of distribution module with valve installed (Line 69).

3.2 Theoretical studies on the gas system

Generally, to characterize a regulation valve, the pressures right before and after the valve are needed. They can be determined starting from constant pressure points of the system and evaluating the different pressure losses until the two points of interest. In this case, as it is possible to see from the schematic of Fig. 3.4 , the two constant pressure points are 0 and 4 and the evaluation of the pressure losses due to the pipe length (0-1) and to the pipe elevation (1-2 and 4-3) is needed. The scheme is a simplified version of the system and pressure losses due to pipe curvatures and other elements present in the system have been neglected.

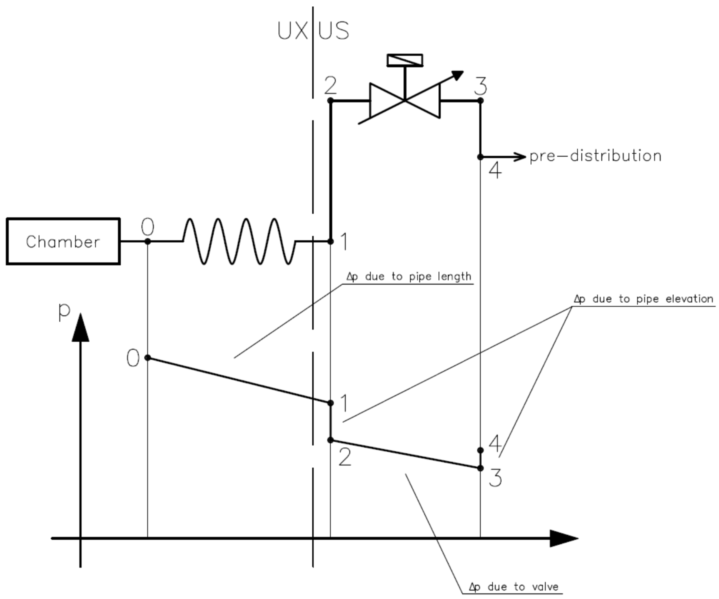

Figure 3.4: Schematic of the gas system studied and its pressure losses.

Once p_1 and p_2 have been determined in the flow rate range in which the system will operate, the next step is to design the valve's seat that generates the Δp needed. To perform this study, the *Ansys* software to run CFD simulations has been used. The results are presented in section 3.4.

3.2.1 Determination of gas mixture's properties

The properties of the gas mixture depend on the concentration of the different gases composing the mixture. These data are listed in Tab. 3.1.

Gas	**Vi**[%]
$C_2H_2F_4$ (R134a)	95.2
i-C_4H_{10}	4.5
SF_6	0.3

Table 3.1: Volume concentrations of the mixture's gases.

The density of the gas mixture is simply evaluated summing the products between the densities of the different gases with their respective volume percentages, therefore following:

$$\overline{\rho} = \sum V_i \rho_i$$

for this specific gas mixture at atmospheric pressure, we obtain a density of about $4.3\,Kg/m^3$. The gas mixture viscosity instead, is calculated with the weights of its constituents, following:

$$\overline{\mu} = \frac{\overline{\rho}}{\sum \frac{V_i \rho_i}{\mu_i}}$$

a viscosity of about $1.36e-5\,Kg/m\,s$ is obtained. Both, the density and the viscosity of the gas mixture were determined at atmospheric pressure and at 20°C. In the following studies, the dependence on temperature and pressure of the gas mixture has been neglected.

3.2.2 Pressure losses evaluation

The pressure loss due to the elevation change can be simply determined following:

$$\Delta p = \Delta \rho z g$$

therefore, the pressure losses between points 1-2 and 3-4 can be quite precisely evaluated. Unfortunately, the pressure loss due to the length of the tube, cannot be evaluated so easily since it is dependent on the flow regime. From [8] 3 different formulas can be used to determine the pressure loss depending on whether the flow regime is laminar (Re<2073), turbulent (Re>3520), or in the intermediate phase. If the flow regime is laminar the pressure loss can be evaluated following:

$$\Delta p = \frac{\overline{\rho} v^2 L}{2D} \frac{64}{\mathfrak{R}}$$

where D is the inner diameter of the pipe, L is the total length of the pipe and v is the average velocity of the gas determined by:

$$v = \frac{Q}{\pi \frac{D^2}{4}}$$

where Q is the volume flowrate. In the equation above $\mathfrak{R}$ stands for the Reynolds number and it is determined as:

$$\mathfrak{R} = \frac{\overline{\rho} v D}{\overline{\mu}}$$

If the flow is turbulent instead, the pressure loss can be evaluated following:

$$\Delta p = \frac{\overline{\rho} v^2 L}{2D} (1.8 \log(\mathfrak{R}) - 1.64)^{-2}$$

While, if the flow regime ends up being in the intermediate zone, the pressure loss can be approximated as:

$$\Delta p = \frac{\overline{\rho} v^2 L}{2D} (k_3 \mathfrak{R}^3 + k_2 \mathfrak{R}^2 + k_1 \mathfrak{R} + k_0)$$

with the coefficients k_3,k_2,k_1 defined in [8].

3.3 Set-up of the simulation

To perform the simulations, the commercial software Ansys has been used. The standard k-epsilon viscous model has been chosen and the resolution method has been set to SIMPLE. In order to obtain accurate results in a reasonable amount of time two studies have been performed: the geometry simplification and the mesh convergence study. These studies are presented in the following and a comparison between experimental data and simulations results is given.

3.3.1 Geometry simplification

The 3D model of the regulation valve was given by the supplier company and the raw fluid volume extracted by it resulted impossible for fluid dynamics simulations purposes mainly because of sharp edges reality incongruences. Therefore, firstly the 3D model and secondly the fluid volume had been adjusted to obtain any result out of a simulation. The resulting simulated fluid volume is shown in Fig. 3.5.

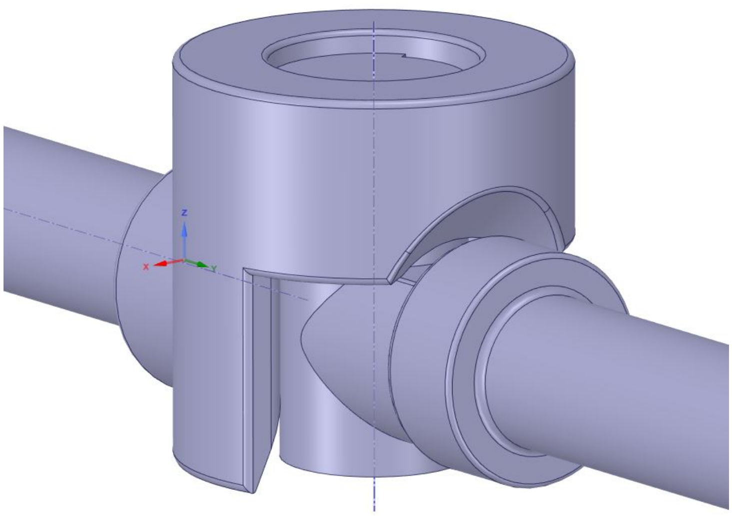

Figure 3.5: Computational fluid volume simplified for the simulations.

3.3.2 Mesh characterization

Meshing is one of the most important steps in performing an accurate simulation using Ansys. A mesh is made up of elements which contain nodes (coordinate locations in space that can vary by element type) that represent the shape of the geometry. The sizing of these elements highly influence the accuracy and the efficiency of a simulation. In the table below (Table 3.2) the sizing parameters used to perform the simulation study are reported. The 3 main sizing parameter families that it was needed to work on are the mesh defeaturing, the capture curvature and the capture proximity. The mesh defeaturing simplify the fluid volume geometry in zones where it is not needed

Use adaptive sizing	No
Growth rate	1.2 m
Max size	1e-2 m
Mesh defeaturing	Yes
Defeature size	2.5e-5 m
Capture curvature	Yes
Curvature min size	5e-5 m
Curvature normal angle	18°
Capture proximity	Yes
Proximity min size	5e-5 m
Num cells across gap	3

Table 3.2: Parameters used to create the main body of the mesh structure

Use automatic inflation	Program controlled
Infaltion option	Smoth transition
Transition ratio	0.272
Maximum layers	5
Growth rate	1.2
Inflation algorithm	Pre

Table 3.3: Parameters used to create the inflation layer of the mesh

such an accuracy e.g. geometrical details that does not affect the fluid dynamical behaviour of the system. The capture curvature parameters provide proper meshing element structures of curvy faces and curvy geometries while the capture proximity parameters give the advantage of defining the minimum element layers between two opposing faces or in an internal volumetric gap. Another important mesh feature that highly improved the simulation efficiency and accuracy is the inflation. The mesh inflation parameters provide a proper treatment of the element structure close to the faces of the fluid volume generating thin cells adjacent to boundaries. In Fig. 3.6 a section of the mesh structure inside the pipeline is reported. It Is possible to see the effect of the mesh inflation on the outer part of the section. In this way the viscous boundary layer equations can be resolved more easily resulting in an increased accuracy of the simulation. The parameters used to create the inflation of Fig. 3.6 are reported in Table 3.3. The smooth transition option has been chosen to maintain smooth volumetric growth between adjacent

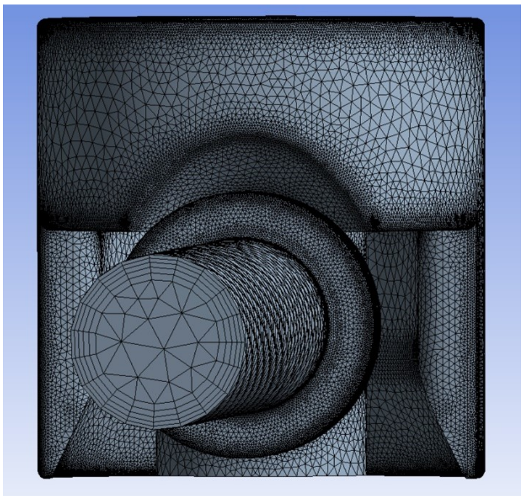

Figure 3.6: Computational fluid volume simplified for the simulations.

layers. In this way, an efficient link between the mesh inflation structure and the rest of the meshing volume was achieved.

Mesh convergence studies

Given the huge number of simulations to be run in a limited period of time, the time efficiency was matter of extreme importance. Since the model equations must be solved for every mesh's cell, the total number of cells determines the computational demand of the simulation. Therefore, the cell size must be appropriate to not have a biased results as well as to avoid time losses. To find the adequate cell size several simulations have been run with different values of this parameter. The results of the study are displayed in the graph below (Fig. 3.7).

Considering that the cell size is inversely proportional to the computational burden of the simulation it was chosen to pursue the studies of the system with a cell size of 5E-3. The two most coarse meshes have not been used because they deviate too much from what is considered the correct result, i.e. the finest mesh result, while the others have been considered too time demanding for the type of work that has to be done. The chosen mesh is displayed in Fig. 3.8.

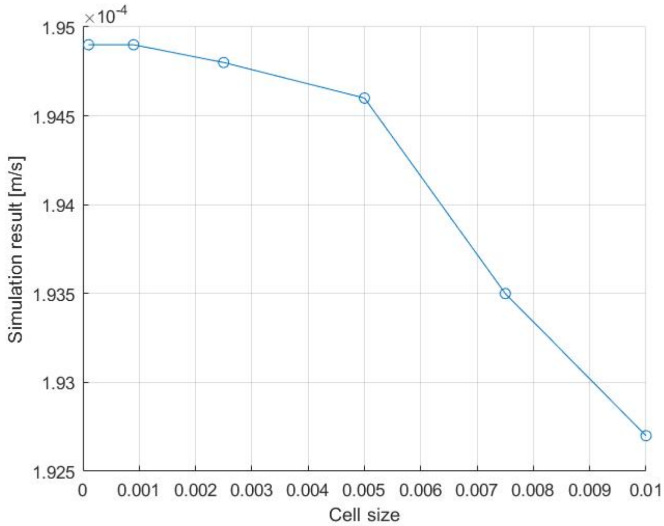

Figure 3.7: Mesh convergence study: result of the simulations over cell size

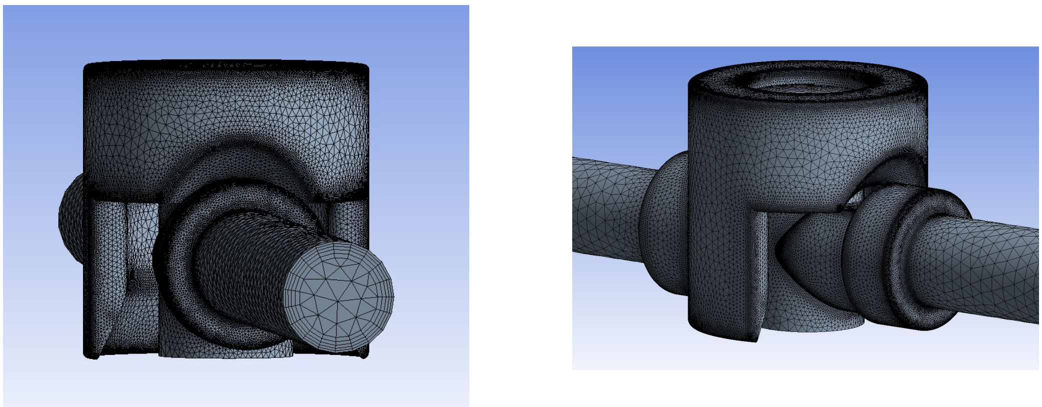

Figure 3.8: Mesh chosen for the studies. Cell size of 5e-3.

3.3.3 Resolution method

To address the turbulences created by the seat of the valve the two equation standard K-epsilon model has been chosen to run the simulations. This model is in general robust and not time consuming as other multiple equation models (as for example the Reynolds stress model) proposed in ANSYS. Furthermore, it very reliable in treating problems where mean pressure gradients are small as in our case. Moreover, since the geometry present several curvy boundaries and narrow sections, the near-wall treatment option non-equilibrium wall functions has been chosen over a standard treatment. In this way, rapid changes of mean flow due to the particular geometry can be properly resolved. Regarding the solution method instead, the Semi-Implicit Method for Pressure-Linked Equations (SIMPLE) was chosen over the coupled method. In general the SIMPLE is less time demanding but the simulations can diverge in case the mesh or the initial guesses are not properly set. Several simulation tests have been carried out and it has been shown that both methods converge to the same value but the computational time with the SIMPLE is about 2/3 the computational time of the coupled method.

3.4 Results and discussion

Following the theory described in Section 3.2, Δp_{12} and Δp_{34} can be easily calculated, Δp_{01} can be evaluated if the flow-rate was known and the flow-rate in certain conditions can be found simulating the flow over the valve if Δp_{23} was known. Therefore, the problem must be solved through an iterative process. In the table below the starting data from the 28 gas lines are listed.

Line	**Flow rate range [l/h]**		$\mathbf{p_0}$ **[mbar]**	$\mathbf{p_4}$ **[mbar]**	$\Delta\ \mathbf{p_{available}}$ **[mbar]**
61	100	210	0.6	-1.5	0.65
62	110	230	1.3	-1.5	1.35
63	110	230	1.3	-1.5	1.35
64	80	160	0.26	-1.5	0.31
65	100	210	2.84	-2.7	3.75
66	110	230	3.5	-2.7	4.41
67	110	230	2.7	-2.7	3.61
68	160	310	3.3	-2.7	4.21
69	440	640	0.1	-2.8	1.35
70	370	610	0.9	-2.8	2.15
71	400	630	2.8	-2.8	1.88
72	420	640	1.1	-2.8	2.35
73	400	620	0.2	-2.8	1.45
74	450	690	3.3	-0.9	2.31
75	380	660	3.3	-0.9	2.31
76	340	640	5.5	-0.9	2.34
77	440	670	3.3	-0.9	2.31
78	440	690	3.3	-0.9	2.31
79	100	210	0.4	-1.8	0.75
80	110	230	2.35	-1.8	2.70
81	110	230	3	-1.8	3.35
82	80	160	0.4	-1.8	0.75
83	100	210	2.5	-2	2.71
84	110	230	2.4	-2	2.61
85	110	230	1.5	-2	1.71
86	160	310	3.35	-2	3.56

Table 3.4: Required flowrate range for every line, pressure of point 0 and 4 of the system and the calculated $\Delta p_{\text{available}}$.

In the first column, the 28 lines are listed following the numeration used in the experiment. The 10 lines going to the BARREL sector are the ones from 69 to 78 while, the others belong to the two ENDCAP sectors. The operational flow-rate ranges and the stable pressure points are reported. While, in the last column, the parameter $\Delta p_{\text{available}}$ is the sum of the two unknown variables: Δp_{01} and Δp_{23}. This parameter, together with the flow-rate range, has been used to divide the 28 lines into groups with similar operating conditions. 4 groups have been created and for each group, a valve's seat has been designed and simulated.

3.4.1 ENDCAP sector designs

Starting from the ENDCAP case, 2 seats have been designed. The first one working in the range of $0.35mbar < \Delta p_{\text{available}} < 1.35mbar$ and the second one of $1.7mbar < \Delta p_{\text{available}} < 4.4mbar$. The results are displayed in the graphs of Fig. 3.9 and the orifice's geometry is shown on the side.

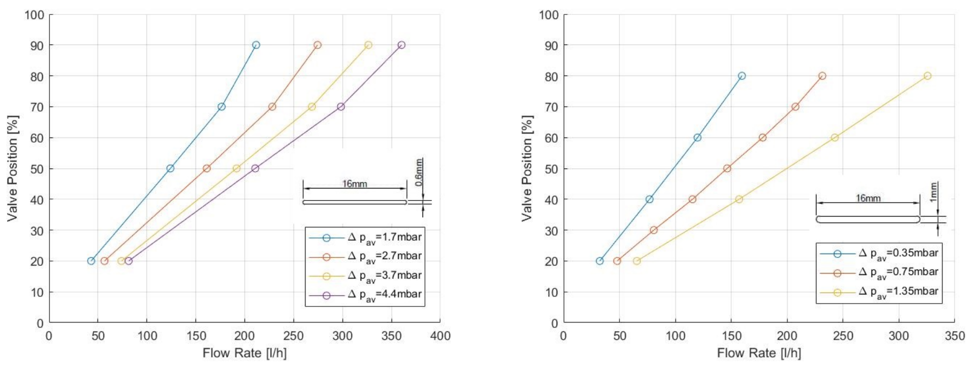

Figure 3.9: Simulations' results of the valve position over the flow-rate at different impedance values for the two designs.

The total orifice areas, i.e. the areas when the valve is fully open (valve position 100%), are respectively $15mm^2$ and $10mm^2$. As we can see from the graphs in figure 12, both designs meet the required flow-rate ranges while working in the valve position range 20-90%. It was decided to not use the full valve range so that in case of extreme pressure oscillations or other operational problems the valve still has some room to regulate the pressure.

3.4.2 BARREL sector designs

Regarding the BARREL case instead, 2 other seats have been designed. One working around a $\Delta p_{\text{available}} = 2.3 mbar$ and one for the lines 69, 71, 73 working at about $\Delta p_{\text{available}} = 1.5 mbar$. As before, the simulations results are displayed in Fig. 3.10.

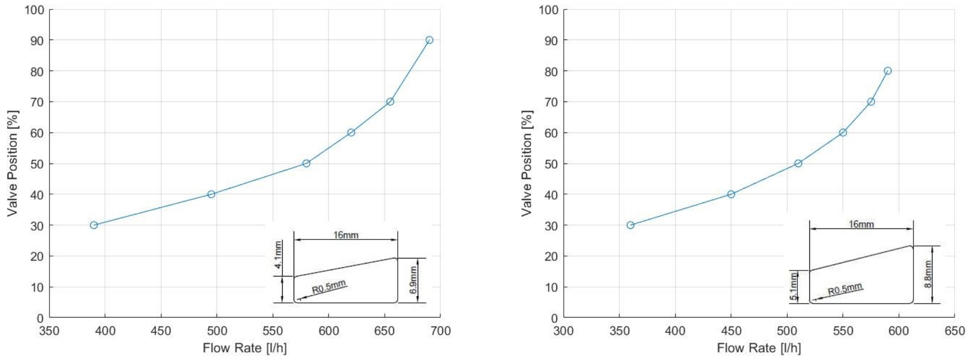

Figure 3.10: Simulations' results of the valve position over the flow-rate for the two designs. On top the seat working at 2.3mbar and on the bottom the seat working at 1.5mbar.

In this case, the orifice's design is not linear since the flow regime is not fully laminar. The trapezoidal shape was instead chosen to meet the increase of pressure losses in the pipelines due to turbulent flow. The design working at $\Delta p_{\text{available}} = 2.3 mbar$ meets the required flow rate ranges and keeps some room for unforeseen problems of under pressure and over pressure. While the other design cannot reach the upper limit of 640 l/h that the lines 69 and 71 require. However, this is not a seat design problem since when the valve is fully open, it does not produce almost any impedance.

3.5 Experimental setup

The seats were tested firstly thank to a lab setup and secondly on the actual system. Two test were performed on the system: the first preparatory test foresees, with the use of the manual regulation valve, to bring the automatic valve from fully open to operational removing step by step the impedance produced by the manual valve. In the second test, the behaviour of the valve at different flow-rates has been explored. To do so, the line's rotameter in the pre-distribution modules has been used. Several tests, in both sectors ENDCAP and BARREL, have been performed to verify the truthfulness of the simulations' results at different flow-rate ranges.

3.5.1 Tests on laboratory setup

The laboratory setup is composed of the automatic valve under test, a compressed air tank, a Mass Flow Controller (MFC), and a pressure transmitter, A photo of the laboratory setup is reported in Fig. 3.11.

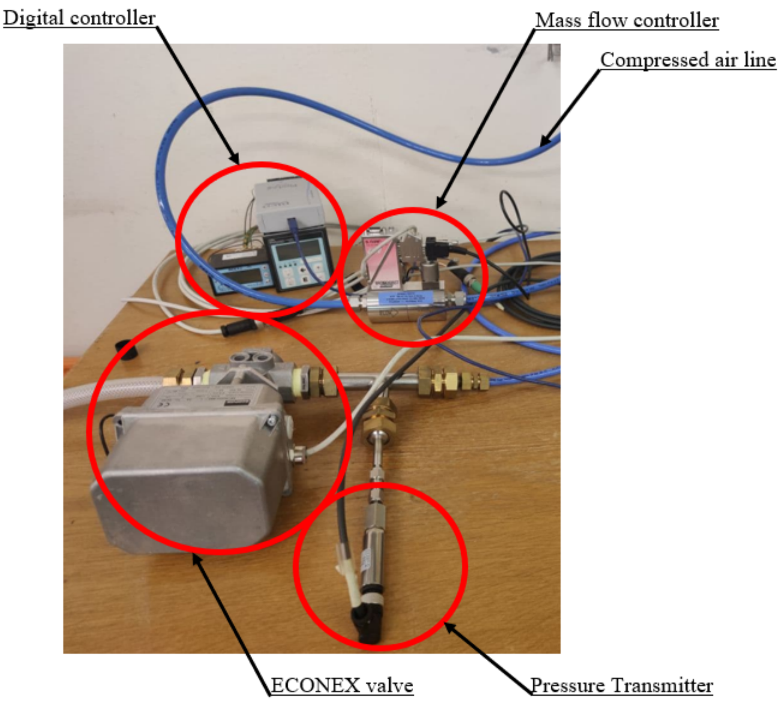

Figure 3.11: Picture of the laboratory setup.

The input of the automatic valve is connected to the compressed air tank, while the output is exhausted to atmosphere.The valve is operated through a digital controller, that allows to set the valve opening position. The MFC device is capable of delivering the desired flow rate to the system and it is controlled via software. The pressure transmitter constantly measures the pressure before the automatic valve, to obtain the value of the impedance across the valve as the downstream pressure is atmospheric. A schematic representation of the laboratory setup is reported in Fig. 3.12.

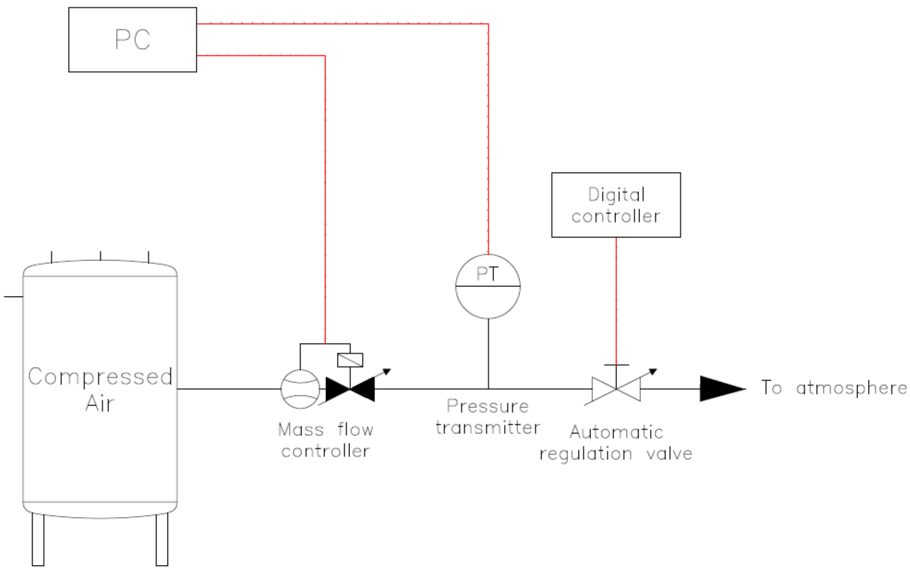

Figure 3.12: Schematic representation of the laboratory setup.

The aim of the laboratory test is to characterize the behavior of the valve for different input gas flow rates, measuring the pressure drop across the valve. The test was performed starting from the valve position with the seat completely open. the seat was rotated in step of 5%, and the impedance was measured, keeping constant the gas flow rate The test was repeated in the same way for different values of the flow rate, that were chosen based on the operational flow of the final setup on the Experiment. Considering that the operational mixture will be mainly R134a and the laboratory test was realized with air, the flow values were calculated with the conversion factor air-gas mixture. To obtain the same flow coefficient over the valve, the air flow rate has to be the double of the gas mixture flow-rate expected in the experiment. As the working behavior of the regulation valve strongly depends on the shape of the internal seat, the same test was realized for three different seat geometries. Fig. 3.13 reports the results obtained from the test of the trapezoidal shape seats with total opening area of 45 mm2, 60 mm2 and 88 mm2. The plots report the impedance of the valve as a function of the valve opening, for two different flow rates (960 l/h and 1920 l/h). It can be seen that for both tested flows, the valve impedance shows an exponential decrease for increasing opening position. It can also be seen that with smaller seat opening areas, the impedance decrease shows and higher slope.

After realizing similar tests on the on-site system, that will be illustrated in details in the following section, it could be concluded that the results of the laboratory tests gave reliable results on the seat impedance even if they were realized in air instead of operational gas mixture. Therefore, it is proved the great advantage of performing this type of test at laboratory level, as compared to a validation on the real-size system, they can be realized much faster hence with the possibility of testing way more configurations in a short span of time.

3.5.2 On-site tests

After the preliminary laboratory tests, the valve was moved on some sample distribution lines on the RPC gas system. The distribution lines configuration was modified to be able to host the automatic valve and connect them to the gas system PLC in order to be controlled via software. In particular, the valves were installed on lines 69, 74 and 83, right before the manual regulation valve on the distribution output lines (Figure 3.3). The three different lines were chosen in way to test the valve impedance in different pressure and flow rate conditions, as they belong to different sectors of the detector system operating hence in different conditions. The automatic valve, when installed, is set 100% open to be in a zero-impedance initial position. One should keep into account that the manual regulation valves, during normal operation, is set to a given impedance to allow the proper regulation of the line pressure. To be able to properly test the automatic regulation, such impedance had to be removed to avoid being influenced by the presence of the manual valve. The first step of the test was therefore to bring the manual regulation at its maximum opening., To do so, the manual valve was lowly opened until end of stroke, with the automatic valve progressively adjusting to compensate the removed impedance. The automatic valve, starting from 100% open, was

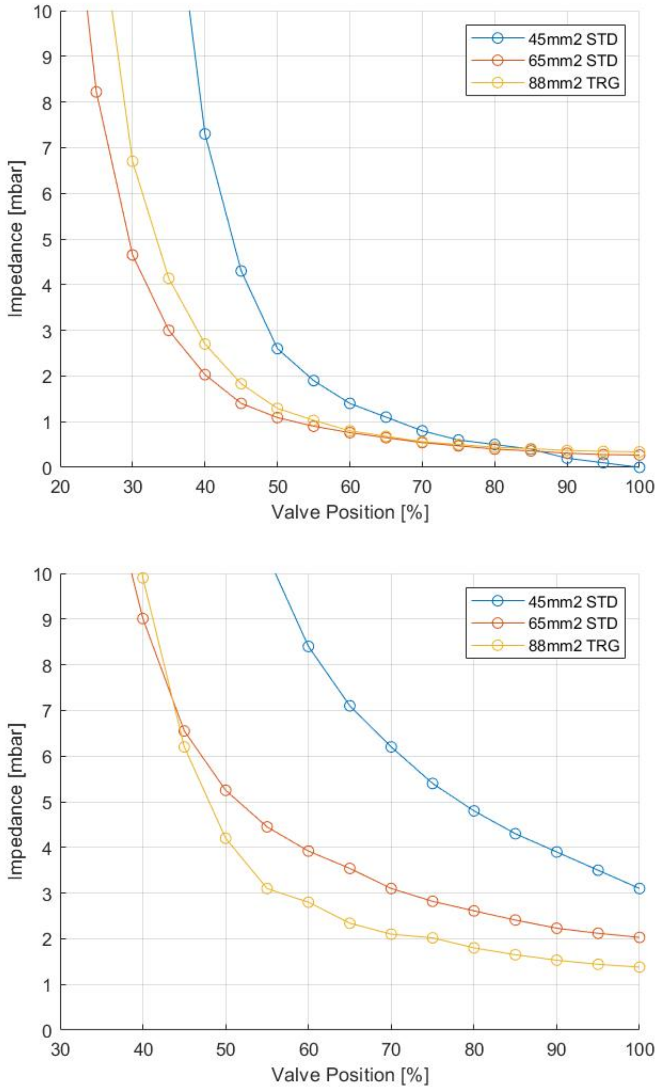

Figure 3.13: Measured impedance of the ECONEX valve for different seat positions and at 960 l/h (top) and 1920 l/h (bottom).

hence closing automatically to keep constant the pressure inside the detector. Fig. 3.14 reports an example of the test, realized on line XX with seat area xx mm2. It shows the automatic regulation valve opening percentage as a function of the position of the manual regulation valve, expressed in degrees of valve knob rotation. A rotation of 0 degrees corresponds to the initial operational position of the manual valve, while 1440 degrees correspond to

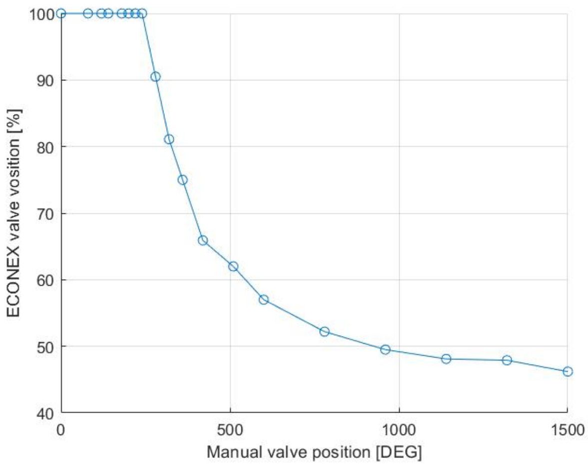

Figure 3.14: Preliminary test example performed in line 74 with a 88 mm2 TRG seat.

the maximum possible opening of the valve. It can be seen from the reported plot that, after an initial range where the rotation of the manual valve has no effect on the line impedance hence no reaction of the automatic valve, the progressive opening of the manual valves causes the progressive closing of the automatic one. After this first step, the manual valve is completely open (no influence on line pressure) and the automatic valve is positioned according to the operational conditions of the line keeping the chamber pressure at 0.00 mbar. The results of these preliminary step of the test were useful to characterize the influence on the system of both valves. It was also noticed that the manual valve can be used to shift the automatic valve operational position towards higher values in case of necessity. Once the manual valve was fully opened, it was possible to test the automatic valve in the flow rate range required by the experiment for each specific line. To do so, the manual mass flow controller (shown in the schematic of Fig. 2.4) placed on the input of each line was used to increase and decrease the flow to cover the full possible flow range of operation. The test was repeated on each line with different seat geometries installed on the valve, to find the optimal one for the specific operation condition. Fig. 3.15 report the results of the test realized respectively on the lines 69 and 74 (belonging to the Endcap section) and on line 83 (belonging to the Barrel section). The valve on line 74 was tested with two different seats, respectively with area of 45 mm2 and 65 mm2, while line

83 was tested with three different seats (15 mm2, 11 mm2, 10 mm2). As expected, in all the realized tests the opening of the automatic valve is found to be increasing for the increase in the total flow rate of operation. It is also found that seats with larger area make it possible to work at a higher flows keeping the opening of the valve at reasonable levels (below 80%).

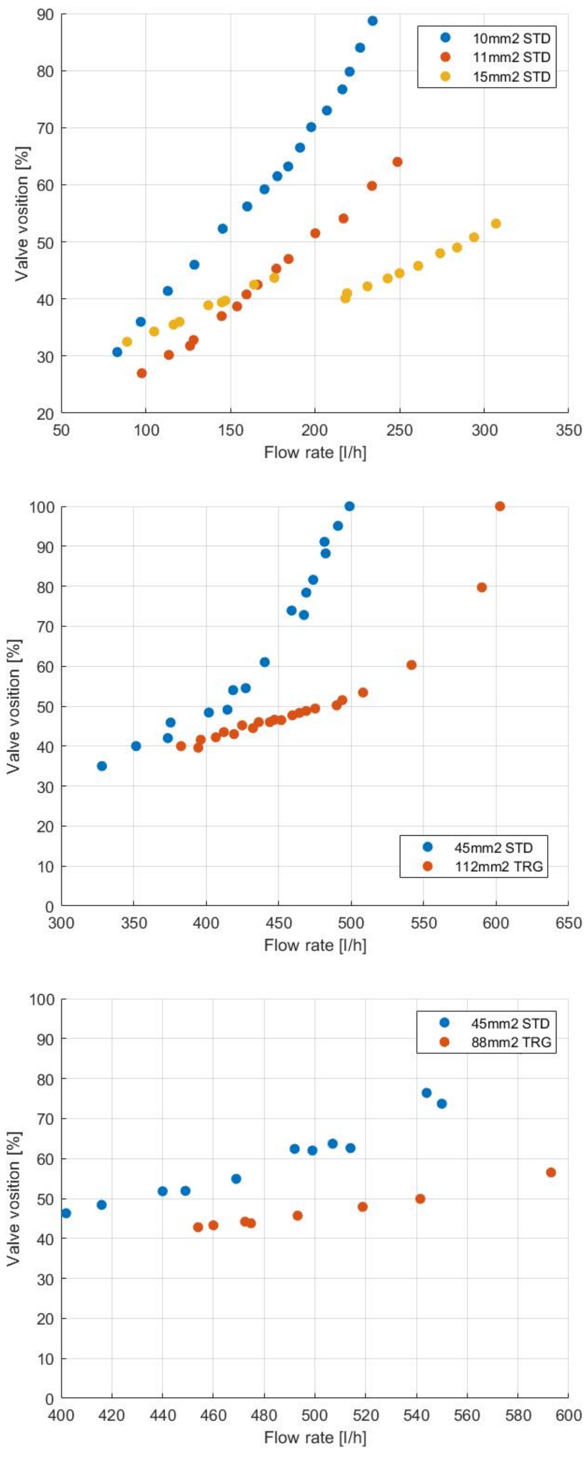

Figure 3.15: Experimental data from tests of different cylinders in line 83 (top), line 69 (middle) and line 74 (bottom).

3.6 Comparison between experimental data and simulation

Once the experimental data phase was over, it was possible to compare the experimental data and the simulation results. In way it was possible to verify the reliability of the simulations performed for the lines with different pressure and flow-rate conditions that were not tested. The comparison between experimental data and simulations is shown in the graphs below (Fig. 3.16). As we can see, the simulations follow the experimental data quite precisely with some errors rising in the regions where the flow regime starts having turbulence, i.e. over 500 l/h.

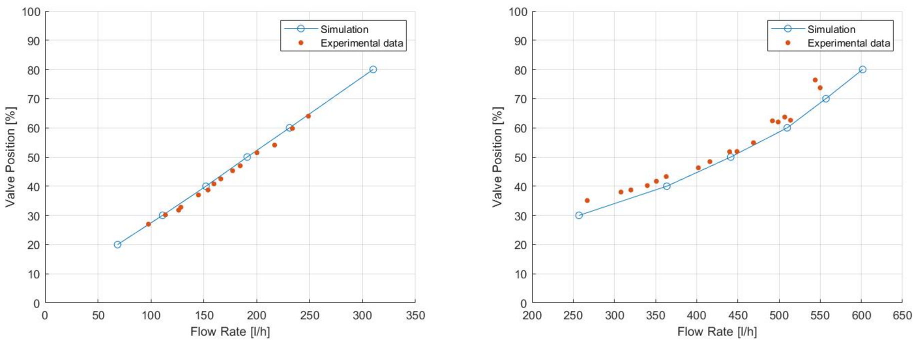

Figure 3.16: Comparison between experimental data and simulations' results. ENDCAP case on the left (Line 83) and BARREL case on the right (Line 74).

3.7 Example of valve operation in presence of system perturbation

One of the main reason why the pressure of the system can drop or oscillate is the purifier module. As introduced in Section 2.3, the purifier module undergoes regeneration cycles, when the flow is switched back to the regenerated volume, the material absorbs a part of the gas mixture until its saturation point. These processes perturb the total flow leading to a system's pressure perturbation as it is possible to see from Fig. 3.17 (curve in green). The perturbation affects in turn the flow-rates of the different lines which result in a drop of pressure in the detector' chambers.

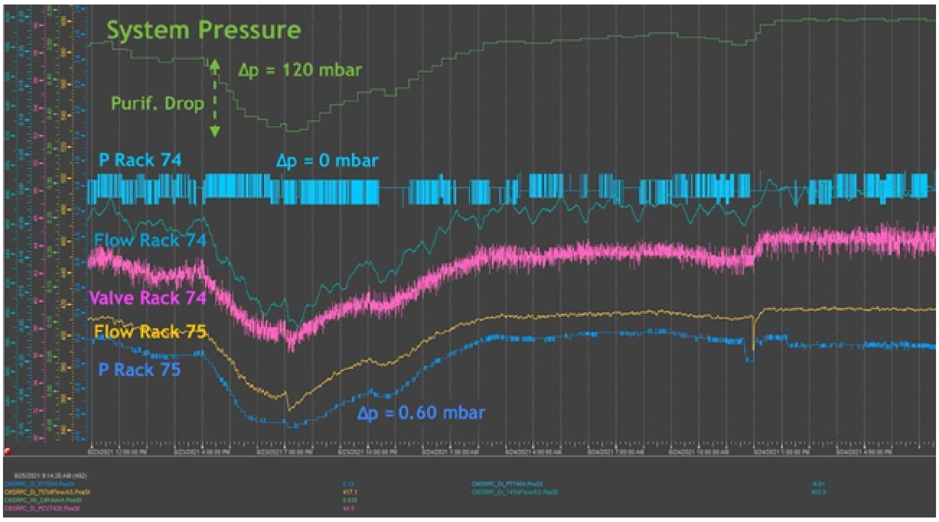

Figure 3.17: Trend of system's pressure and lines 74 and 75 flow-rates and pressures from the CERN gas system control software. Comparison between line 74 (with valve) and line 75 (without valve) during a system pressure perturbation.

In Fig. 3.17, two gas lines (74 and 75) are compared. One regulation valve is installed on line 74, while line 75 does not have any regulating device. It can be to noticed that, when the flow drops in line 75, the chamber's pressure falls of about $0.6mbar$. Meanwhile, when the flow drops in line 74, the valve instantly acts and the detector's pressure is not affected at all by the system perturbation. Such a pressure drop inside the detector's chamber could be dangerous and could result in the break of the connectors or connecting pipes, therefore, the valve plays a crucial role during these situations.

3.8 Different operational conditions

During long shutdowns the detector can be flushed with air to avoid using GHG or expensive gases. Since air has different properties it produces different impedance resulting in a drift of the chambers' pressure while switching from mixture to air or the opposite. Until now, to maintain the pressure constant, every time the operational conditions change, the pressure was kept stable with the use of a manual valve however, this process is complicated and time demanding. In order to automatize the procedure a study on how the valve behaves with air and with 50% air - 50% gas mixture have been performed. In Fig. 3.18 the results of the simulations are shown.

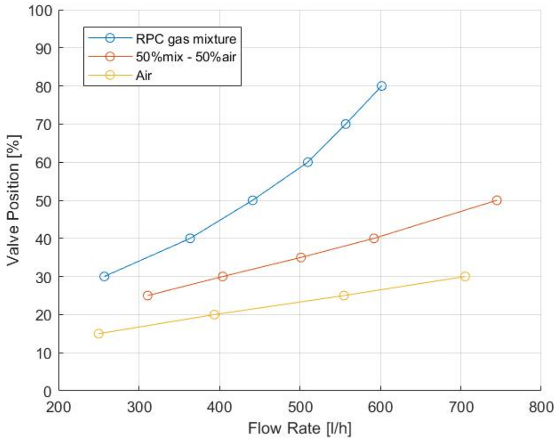

Figure 3.18: Example of the valve position over flow-rate curve behaviour with different gases.

As we can see from the graph above, the valve operational curve is drifted towards smaller valve position percentages but the valve still manages to regulate in the same flow-rate range. This study shows how the designed seats would react to such an operational change and why it is important to design the seat for an operational valve position range above 20%-30%.

Chapter 4

Conclusion

In this thesis work, a detailed study of the gas system that provides the gas mixture to the CMS RPC detector has been performed. Given the fragility of pipes and connectors between the detectors and the gas system, it is fundamental to minimise any pressure and flow-rate perturbation.

In order to do so, it was decided to add automatic regulation valves on the system, programmed to keep the chambers' pressure stable despite any system perturbation. The seat of these valves can be customised to meet the required pressure and flow-rate ranges. CFD simulations were performed to study the seat geometry that best suits the conditions of the system. For the 28 gas lines in which the valves were foreseen, 4 seat's designs have been considered optimal to meet the different requirements of each line. Therefore, they have been 3D printed in CERN and the valves were tested both in a laboratory set-up and on the actual RPC gas system. These tests provided the data to confirm the reliability of the simulations, thus the studies have been approved and the valves validated. The installation on 28 regulation valves is foreseen for the end of 2021 in order to be operative for the next LHC Run 3 expected in Spring 2022.

Bibliography

[1] *Standard Model*. URL: https://en.wikipedia.org/wiki/Standard_Model.

[2] Christiane Lefèvre. *The CERN accelerator complex*. Apr. 2010. URL: https://cds.cern.ch/record/1260465.

[3] Mara Corbetta. "Development of Gas Systems for Gaseous Detector Operation at HL-LHC". PhD thesis. UNIVERSITÉ DE LYON, 2020, p. 162.

[4] Glenn F Knoll. *Radiation detection and measurement*. 2010. URL: https://cds.cern.ch/record/1300754.

[5] Nevis Columbia. *Resistive Plate Chambers*. 2015. URL: https://www.nevis.columbia.edu/~chi/rpc/cms-rpc-tech-note.pdf.

[6] Gianluca Rigoletti. "Performance studies on Resistive Plate Chambers detectors operated with new environmentally friendly gas mixtures at CERN GIF++ facility". MA thesis. UNIVERSITÁ DEGLI STUDI MILANO-BICOCCA, 2019, p. 83.

[7] Christiane Lefèvre. *The CMS experiment*. 2010. URL: https://cds.cern.ch/record/1260465.

[8] *Formulas for pressure drop calculations*. 2010. URL: https://detector-gas-systems.web.cern.ch//Tools/deltaPformulae.htm.